CrystEngComm

RSC Publishing

PAPER

View Article Online
View Journal

Crystal structures and binding studies of atovaquone and its derivatives with cytochrome bc_1: a molecular basis for drug design†

Cite this: DOI: 10.1039/c3ce40336j

Susanta K. Nayak,[a] Srijita Basu Mallik,[a] Shankar Prasad Kanaujia,[b] Kanagaraj Sekar,[b] K. R. Ranganathan,[c] V. Ananthalakshmi,[c] G. Jeyaraman,[c] S. S. Saralaya,[d] K. Sundararaja Rao,[d] K. Shridhara,[d] K. Nagarajan*[d] and Tayur N. Guru Row*[a]

Received 23rd February 2013,
Accepted 31st March 2013

DOI: 10.1039/c3ce40336j

www.rsc.org/crystengcomm

Crystal structure of *trans*-atovaquone (antimalarial drug), its polymorph and its stereoisomer (*cis*) along with five other derivatives with different functional groups have been analyzed. Based on the conformational features of these compounds and the characteristics of the nature of intermolecular interactions, valuable insights into the atomistic details of protein–inhibitor interactions have been derived by docking studies. Atovaquone and its derivatives pack in the crystal lattice using intermolecular O–H···O hydrogen bond dimer motifs supported by surrogate weak interactions including C–H···O and C–H···Cl hydrogen bonds. The docking results of these molecules with cytochrome bc_1 show preferences to form N–H···O, O–H···O and O–H···Cl hydrogen bonds. The involvement of halogen atoms in the binding pocket appears to be significant and is contrary to the theoretically predicted mechanism of protein–ligand docking reported earlier based on mimicking experimental binding results of stigmatellin with cytochrome bc_1. The significance of subtle energy factors controlled by weak intermolecular interactions appears to play a major role in drug binding.

Introduction

Malaria is caused by a parasite and is affecting several regions on the globe which include tropical and sub-tropical regions of Africa, Asia and parts of the Americas.[1–3] The treatment of malaria was initially based on the extraction of quinines from the barks of cinchona,[4] however over the years a whole range of anti-malarial drugs have been discovered and used effectively on patients. In recent years, the parasite has developed resistance to most of the drugs demanding the requirement of newer and better drugs[5] and the approach is to attack the parasite *via* different metabolic pathways. Quinine and its derivatives like amodiaquine, mefloquine and primaquine[6] act on food vacuole[7–9] whereas chloroquine[10–12] and artemisinin[13] act *via* different mechanisms leading to parasitic cell death.[14] Artemisinin acts as a redox drug in which the peroxy linkage gets reduced leading to the drug molecule acting as a good oxidizing agent in the redox cycle.[15] Sulpha drugs act with a mechanism of inhibiting the folate synthesis, thus, reducing the possibility of mutation of the parasite.[16,17]

Among the new generation drugs, atovaquone (2-[*trans*-4-(4′-chlorophenyl)cyclohexyl]-3-hydroxy-1,4-hydroxy naphthoquinone) has shown a broad spectrum activity and based on the structural similarity with ubiquinol appears to bind to cytochrome bc_1 complex.[26] Indeed, atovaquone acts as a ubiquinone inhibitor in the mechanism of mitrochondrial respiration.[18,19] The mitrochondrial electron transfer occurs through several consecutive redox reaction in which the quinine group of ubiquinone get reduced to quinol.[20,21] Likewise, the quinine group of atovaquone can mimic ubiquone[22] while binding to the ubiquinol oxidation pocket of the cytochrome bc_1 complex.[22,23] It has been demonstrated that the stigmatellin[24] binds selectively to the cytochrome bc_1 complex hydroxyl group to Glu272 of cytochrome *b* on one hand and with carbonyl group to His181 of the Rieske iron–sulfur protein on the other[25] of cytochrome *b*. Since, it is presumed that atovaquone also binds in a similar manner to that of stigmatellin an energy minimized structure of atovaquone has been generated in the ubiquinol oxidation pocket assuming the cytochrome bc_1 complex.[26] In recent times, several applications of atovaquone drug, its develop-

[a]*Solid State and Structural Chemistry Unit, Indian Institute of Science, Bangalore 560012, India. E-mail: ssctng@sscu.iisc.ernet.in; Fax: +91-80-2360 1310; Tel: +91-80-2293 2796*
[b]*Bioinformatics Centre, Indian Institute of Science, Bangalore 560012, Karnataka, India*
[c]*KOP Research Centre, Bangalore 562106, Karnataka, India*
[d]*Alkem Laboratories Limited R & D Centre, Bangalore 560058, Karnataka, India*

† Electronic supplementary information (ESI) available: The synthesis procedures adopted and melting points (Table S1), Fig. S1–S6. CCDC 749765–749772. For ESI and crystallographic data in CIF or other electronic format see DOI: 10.1039/c3ce40336j

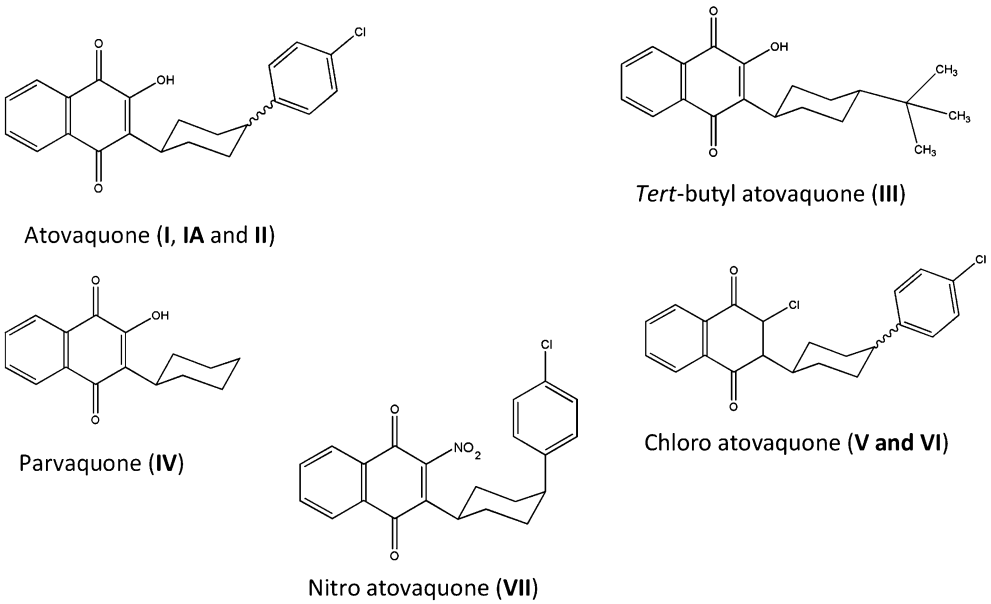

Scheme 1 (**I**) Atovaquone [Form I] and (**IA**) Atovaquone [Form II] = 2-[*trans*-4-(4′-chlorophenyl)cyclohexyl]-3-hydroxy-1,4-hydroxy naphthoquinone. (**II**) *cis*-atovaquone = 2-[*cis*-4-(4′-chlorophenyl)cyclohexyl]-3-hydroxy-1,4-hydroxy naphthoquinone. (**III**) *tert*-Butyl atovaquone = *trans*-2-(4-*tert*-butylcyclohexyl)-3-hydroxynaphthalene-1,4-dione. (**IV**) Parvaquone = 2-cyclohexyl-3-hydroxynaphthalene-1,4-dione. (**V**) *trans*-Chloro atovaquone = *trans*-2-(4-(4′-chlorophenyl)cyclohexyl)-3-chloronaphthalene-1,4-dione. (**VI**) *cis*-Chloro atovaquone = *cis*-2-(4-(4′-chlorophenyl) cyclohexyl)-3-chloronaphthalene-1,4-dione. (**VII**) Nitro atovaquone = *cis*-2-(4-(4′-chlorophenyl)cyclohexyl)-3-nitronaphthalene-1,4-dione.

ment, delivery and efficiency of biological activity have emerged as interesting topics of research.[50]

The molecular basis of protein–ligand interactions can be studied in two ways, one by mutational studies on the protein molecule[26b] and the second by modifying different functional groups of the ligand molecules. Structure-based approach towards the search for a potential inhibitor seems to be a promising technique of the modern era.[27] In the present study, the crystal structure of atovaquone, a potential inhibitor of cytochrome bc_1 complex has been solved in two forms (**I**, **IA**) including one stereoisomer, *cis*-atovaquone (**II**). In addition, crystal structures of five derivatives, *tert*-atovaquone (**III**), parvaquone (**IV**), *trans*-chloro atovaquone (**V**), *cis*-chloro atovaquone (**VI**) and nitro atovaquone (**VII**) of different functional groups have also been solved (Scheme 1). Atovaquone and its derivatives exhibit diverse biological activity.[5] The idea here is to obtain several possible conformational features associated with the ligand to evaluate the nature of binding with the protein molecule. Furthermore, based on the conformational features of these compounds, the characteristics of the nature of hydrogen bonding and other weak intra and intermolecular interactions, the docking studies provide a valuable insight into the atomistic details of protein–inhibitor interactions. The docking study of atovaquone and its derivatives with the ubiquone oxidation domain of the protein molecule reveals a common hydrogen bonding pattern. Since the conformation of atovaquone and its derivatives have been determined using single crystal X-ray diffraction, it is worthwhile evaluating the binding pattern with model systems. These studies also serve to provide inputs for drug design based on the nature of intermolecular interactions.

Experimental

Synthesis and crystallization

The synthesis of atovaquone (**I–VI**) was based on the procedure described in the literature.[28,29] All the synthesis procedures and for the new compound nitro atovaquone (**VII**) have been provided in the ESI.† The single crystals suitable for X-ray diffraction were grown by slow evaporation methods. All the crystals were grown at room temperature except for the crystal **VII** which was crystallized at 0 °C. Crystals of **I**, **V**,[49] **VI**, and **VII** were obtained from the solvents methylene chloride and hexane (2 : 1, v/v), whereas **IA** was obtained from acetone and water (2 : 1, v/v) and **II**, **III**, and **IV** were obtained from acetone solvent. The morphological difference was observed in the case of the polymorphic form of *trans*-atovaquone *i.e.* block and plate shaped crystals for **I** and **IA** forms of atovaquone respectively (Fig. S2, ESI†).[49] It has also been reported earlier that DSC measurements and thermodiffractometry analyses on polycrystalline batches showed crystal-to-crystal interconversion of these forms upon heating at 210(2) °C.[49]

Crystal structure determination

X-ray diffraction data were collected on Bruker AXS with a SMART APEX CCD diffractometer. The X-ray generator was operated at 50 kV and 35 mA, using Mo Kα (λ = 0.7107 Å) radiation and a graphite monochromator. Data were collected for 606 frames per set by using SMART with different settings of φ (0°, 90°, 180°) for compounds (**I**, **IA**, **IV**, **V** and **VI**) and φ (0°, 90°, 180°, 270°) for (**II**, **III** and **VII**) keeping the sample to detector distance of 6.062 cm and the 2θ value fixed at −25°. Data reduction and analysis were performed by SAINTPLUS, XPREP and SADABS.[30] Structures were solved and refined by

Table 1 Crystallographic details

	trans-Atovaquone (**I**)	*trans*-Atovaquone (**IA**)	*cis*-Atovaquone (**II**)	*tert*-Butyl atovaquone (**III**)
Formula	$C_{22}H_{19}O_3Cl$	$C_{22}H_{19}O_3Cl$	$C_{22}H_{19}O_3Cl$	$C_{20}H_{24}O_3$
CCDC No.	749766	749765	749767	749768
Formula weight	366.8	366.8	366.8	312.4
Crystal system	Monoclinic	Monoclinic	Monoclinic	Triclinic
Space group	$P2_1/n$	$P2_1/c$	$P2_1/c$	P-1
a (Å)	5.937(1)	12.548(2)	13.251(1)	5.950(1)
b (Å)	18.357(2)	5.267(1)	10.928(1)	12.479(2)
c (Å)	16.669(2)	27.848(5)	12.630(1)	12.977(2)
α (°)	90	90	90	107.582(2)
β (°)	97.334(2)	92.573(3)	95.450(1)	100.950(2)
γ (°)	90	90	90	103.635(2)
Volume (Å^3)	1801.94(6)	1838.39(6)	1820.84(3)	856.55(11)
Z	4	4	4	2
Density (g cm^{-3})	1.35	1.33	1.34	1.21
μ (mm^{-1})	0.231	0.226	0.229	0.080
F(000)	767.9	767.9	767.9	336.0
$\theta_{min,max}$ (°)	1.7, 26.0	1.6, 25.0	1.5, 26.0	1.7, 25.0
$h_{min,max}$	−7, 7	−14, 14	−16, 16	−7, 7
$k_{min,max}$	−22, 22	−6, 6	−13, 13	−14, 14
$l_{min,max}$	−20, 20	−33, 33	−15, 15	−15, 15
No. of meas. refln.	18 409	16 569	18 281	8342
No. of unique refln.	3514	3237	3572	3004
No. of parameters	311	311	311	260
R_{all}, R_{obs}	0.127, 0.055	0.184, 0.089	0.051, 0.039	0.156, 0.097
w$R_{2,all}$, w$R_{2,obs}$	0.106, 0.082	0.158, 0.131	0.110, 0.099	0.316, 0.272
$\Delta\rho_{min,max}$ (e Å^{-3})	0.171, −0.156	0.272, −0.193	0.160, −0.230	0.462, −0.232
G.o.f	1.019	1.121	1.036	0.955

	Parvaquone (**IV**)	*trans*-Chloro atovaquone (**V**)	*cis*-Chloro atovaquone (**VI**)	Nitro atovaquone (**VII**)
Formula	$C_{16}H_{12}O_3$	$C_{22}H_{18}O_2Cl_2$	$C_{22}H_{18}O_2Cl_2$	$C_{22}H_{18}O_4NCl$
CCDC No.	749769	749770	749771	749772
Formula weight	252.3	385.3	385.3	395.8
Crystal system	Monoclinic	Monoclinic	Triclinic	Triclinic
Space group	$P2_1/n$	$P2_1/n$	P-1	P-1
a (Å)	14.401(3)	10.367(1)	5.977(2)	11.751(2)
b (Å)	5.328(1)	7.051(1)	12.226(4)	12.799(2)
c (Å)	17.393(3)	25.102(2)	13.102(4)	13.985(2)
α (°)	90	90	103.814(5)	75.766(3)
β (°)	98.926(3)	99.777(2)	90.038(5)	67.022(2)
γ (°)	90	90	95.271(5)	83.020(3)
Volume (Å^3)	1318.42(7)	1808.39(7)	925.56(14)	1876.45(23)
Z	4	4	2	4
Density (g cm^{-3})	1.27	1.41	1.38	1.40
μ (mm^{-1})	0.088	0.373	0.364	0.233
F(000)	527.9	799.9	400.0	823.9
$\theta_{min,max}$ (°)	1.7, 25.0	1.6, 26.0	1.6, 25.0	1.6, 25.0
$h_{min,max}$	−17, 17	−12, 12	−7, 7	−13, 13
$k_{min,max}$	−6, 6	−8, 8	−14, 14	−15, 15
$l_{min,max}$	−20, 20	−27, 30	−15, 15	−16, 16
No. of meas. refln.	9080	13 553	6683	13 653
No. of unique refln.	2334	3542	3241	6565
No. of parameters	236	307	307	649
R_{all}, R_{obs}	0.081, 0.049	0.146, 0.064	0.086, 0.054	0.135, 0.052
w$R_{2,all}$, w$R_{2,obs}$	0.163, 0.137	0.114, 0.090	0.156, 0.137	0.118, 0.089
$\Delta\rho_{min,max}$ (e Å^{-3})	0.159, −0.123	0.233, −0.216	0.495, −0.203	0.188, −0.165
G.o.f	0.883	1.032	1.025	0.945

using SHELXL97[31] in the program suite WinGX.[32] The molecular diagrams were generated using ORTEP-3[33] and the packing diagrams were generated using CAMERON.[34] The geometric calculations were carried out by PARST95[35] and PLATON.[36] Non-hydrogen atoms were refined anisotropically and hydrogen atoms bonded to C and O atoms were located from difference Fourier maps and refined isotropically. Table 1 lists the details of crystallographic information and refinement of all compounds.

Docking studies

All compounds were subjected to automated docking simulation using the program AutoDock 3.0.5.[37] AutoDock program is based on a Lamarckian genetic algorithm (LGA) method. Basically, this program determines total interaction energies

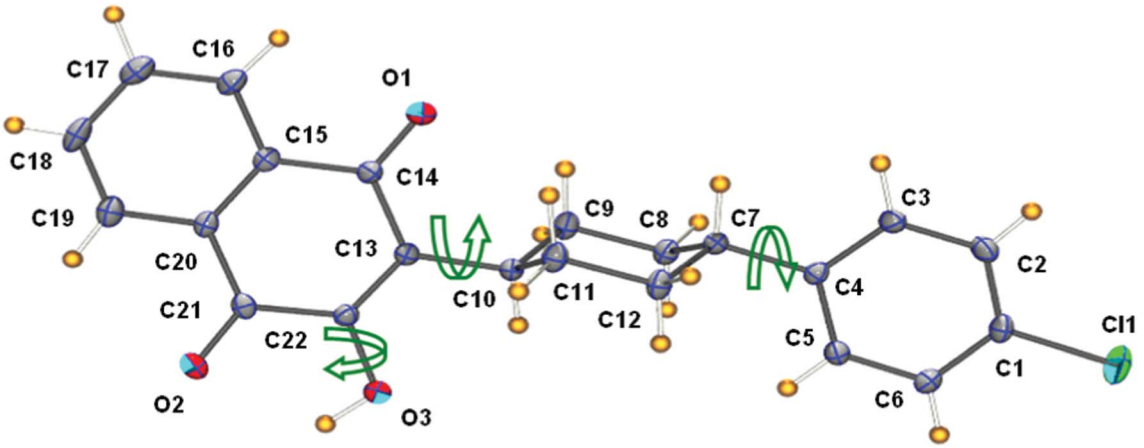

Fig. 1 ORTEP diagram of atovaquone (**I**) with numbering scheme and the allowed rotatable bonds are highlighted as green arrows used in the docking study.

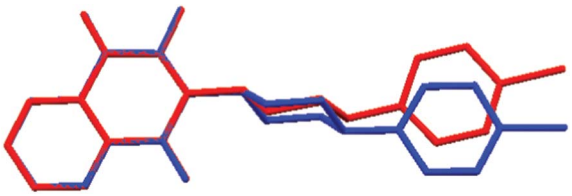

Fig. 2 Overlay diagram depicting the molecular conformational differences of polymorphs of atovaquone, red colour (**I**) and blue colour (**IA**) with respect to the naphthoquinone ring.

between random pairs of ligands and various selected portions of protein to determine docking poses. The three-dimensional atomic coordinates of cytochrome bc_1 were taken from the crystal structure of cytochrome bc_1 + stigmatellin (PDB id: 1EZV) complex by excluding stigmatellin.[38] All the crystallographic water molecules except one were removed from the protein molecule. The three-dimensional atomic coordinates of the ligand molecules were prepared using WinGX.[32] The ligand molecule was placed in a similar manner as stigmatellin in the case of cytochrome bc_1 using the modeling program COOT.[39] The water molecule was fixed at a hydrogen bonding distance of 2.61 Å from OE2 atom of Glu272, which has the potential to form a hydrogen bond with the ketonic group of ligand molecule as indicated in the previous studies.[26] Hydrogen atoms were added to the ligand molecule using the web-server PRODRG.[40] The Kollman charges were added to the protein atoms and the ligand atoms were assigned the Gasteiger partial charges using the program AutoDock.[37] The solvation parameters were added using the addsol module of AutoDock. Three rotatable bonds (C4–C7(1), C10–C13(2) and C22–O3(3)) were allowed to change in the optimization of the prescribed conformation of the ligand molecule (Fig. 1). A grid box of 60 × 60 × 60 points in x, y, and z dimensions were used with a grid spacing of 0.375 Å. The grid was automatically centered at the centre of mass of the ligand molecules modeled in the active site. The electrostatic map and atomic interaction maps for all atom types of the ligand molecules were calculated using the autogrid module of the program AutoDock. The docking simulations were allowed to run for 250 runs using a Lamarckian genetic algorithm for global and a Solis & Wets algorithm for local searches with an initial population size of 250.[41,42] The default values for the maximum number of generations (27 000) and energy evaluations (2 500 000) were taken for the simulations. Additional docking parameters like elitism (1), mutation rate (0.02), crossover rate (0.8) and local search rate (0.06) were taken as the default values implemented in the program. Final docked conformations of the ligand molecules in the active site were clustered using a tolerance of 1 Å of root-mean-square deviations (RMSD). The final conformers were selected based on the binding characteristics and energy in the active site of the protein molecule. The docking energies for the best conformers are given in Table 5. PyMOL[43] is used for both viewing and drawing purposes. All

Table 2 Selected torsion angles ϕ (°) for all compounds

Compound (ϕ) as (°)	C7–C12–C11–C10	C12–C11–C10–C9	C11–C10–C9–C8	C10–C9–C8–C7
I	−55.1(3)	57.4(3)	−57.3(3)	55.5(4)
IA	−55.8(5)	52.6(5)	−52.9(5)	55.6(5)
II	−52.0(2)	51.5(2)	−56.2(2)	59.5(2)
III	56.2(5)	−56.3(4)	55.1(5)	−54.8(5)
IV	54.7(3)	53.9(3)	54.7(3)	54.7(3)
V	−55.7(1)	−53.30(3)	77.7(1)	−55.5(1)
VI	58.9(1)	58.9(1)	−60.4(3)	59.7(1)
VII	−56.7(4)	58.4(4)	−59.8(4)	58.8(1)

Table 3 The dihedral angle (°) between the least squares planes for all compounds[a]

Compound	Plane (1)–plane (2)	Plane (1)–plane (3)	Plane (2)–plane (3)
I	89.23(9)	11.73(6)	77.92(7)
IA	86.78(3)	4.89(1)	88.60(10)
II	78.92(6)	65.57(4)	87.40(5)
III	65.74(9)	80.72(8)	86.89(8)
IV	—	—	85.08(6)
V	89.90(1)	14.63(1)	77.69(10)
VI	66.08(1)	83.15(9)	85.01(8)
VII	65.74(9)	80.72(8)	86.89(8)

[a] Where plane (1) = C1–C2–C3–C4–C5–C6, plane (2) = C7–C8–C9–C10–C11–C12, plane (3) = C13–C14–C15–C16–C17–C18–C19–C20–C21–C22.

the figures were drawn keeping the ligand molecule in the active site of the cytochrome bc_1 complex.

Results and discussions

Crystal structure determination and conformational features

Structures (**I** and **IA**): atovaquone crystallizes in the space group $P2_1/n$ (**I**) using acetone solvent whereas, in acetone and water mixture, it crystallizes in $P2_1/c$ (**IA**) with $Z = 4$. Fig. 1 and S1, ESI,† show that both the structures appear in "extended" conformation due to the formation of intramolecular hydrogen bonds. The basic difference between the two polymorphs is in their conformation as shown in Fig. 2, thus generating conformational polymorphism.[49] Tables 2 and 3 list the selected torsion angles and angles between the least square planes passing through the ring system, respectively, which clearly suggest their conformational differences. The most significant feature is the formation of O–H···O hydrogen bonded dimers across the centre of symmetry in each case (Fig. 3 and Table 4). Furthermore, an additional C–H···O hydrogen bond (again as dimers) dictates the nature of packing of the molecule in the unit cell. The melting point difference between the two forms as seen from Differential Scanning Calorimetry (DSC) studies (Fig. S3, ESI†) is nearly 7 °C proving the occurrence of polymorphism.

cis-Atovaquone (**II**), *tert*-butyl atovaquone (**III**) and parvaquone (**IV**) also crystallize in centrosymmetric space groups with a well defined dimer of O–H···O hydrogen bonds across the centre of symmetry (Table 4). This feature appears to be dominant in atovaquone derivatives with the O–H group in the naphthoquinone moiety. It is expected that the binding studies should have this feature as a structure directing influence. Structure (**II**) has in addition C–H···Cl, C–H···O and π···π intermolecular interactions (Table 4). The *cis* configuration ensures the formation of π···π stack rendering the molecules to have a significantly different conformation (Tables 2 and 3). The ORTEP and packing diagram of structures **II**, **III**, and **IV** are given in Fig. 4 and 5, respectively.

Structures of *trans*-chloro (**V**) and *cis*-chloro atovaquone (**VI**) replace the O–H group of naphthoquinone ring by chlorine,

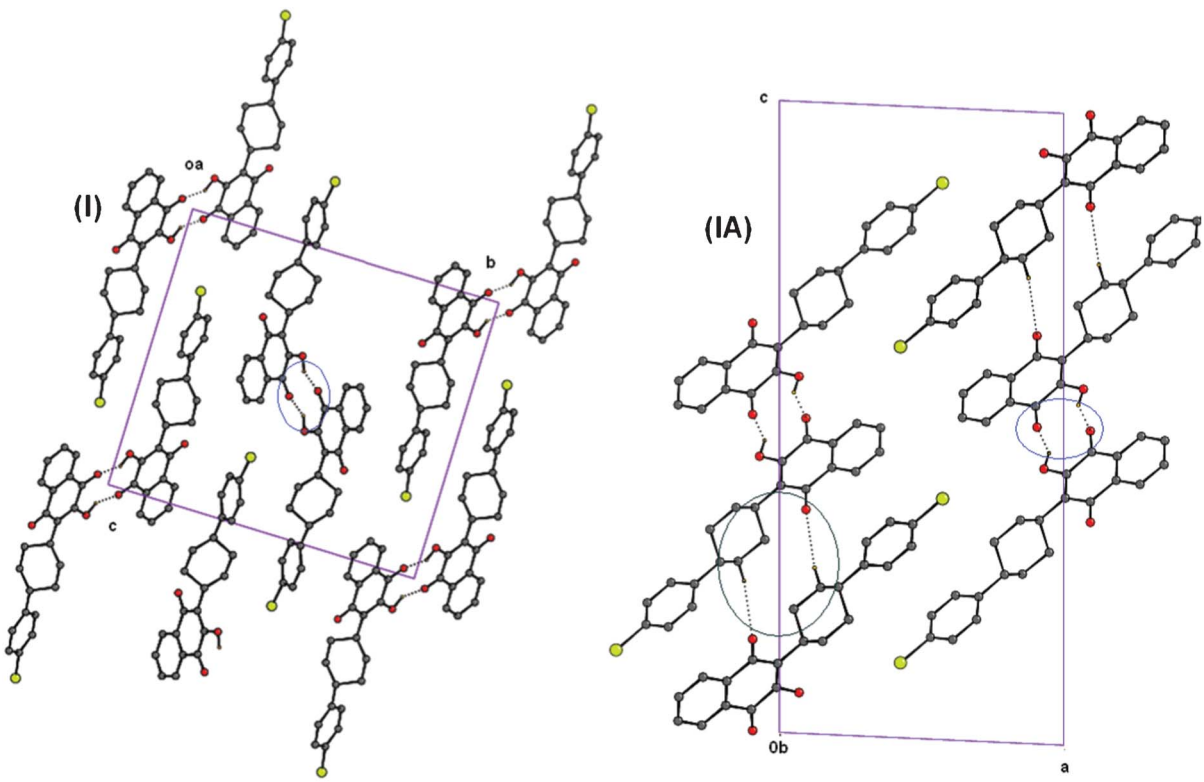

Fig. 3 Packing diagrams of atovaquone (**I**) and (**IA**) are depicting O–H···O hydrogen bonded dimers (highlighted as blue circle) across the center of symmetry and additional weak C–H···O hydrogen (green circle) stabilizing the molecular packing for polymorph form (**IA**).

Table 4 Intra and intermolecular interactions[a]

Crystal	D–H···A	D···H/Å	D···A/Å	H···A/Å	∠D–H···A/°	Symmetry
I	O3–H30···O2	0.92(3)	2.66(2)	2.11(3)	117	x, y, z
	C11–H11A···O1	0.98(2)	3.014(3)	2.44(2)	116	x, y, z
	O3–H30···O2	0.92(3)	2.784(3)	2.03(3)	138	$1 - x, 1 - y, 1 - z$
IA	O3–H30···O2	0.89(5)	2.642(4)	2.14(5)	115	x, y, z
	C11–H11A···O1	0.92(4)	3.130(5	2.58(4)	119	x, y, z
	C9–H9A···O1	1.05(4)	3.128(6)	2.42(4	124	x, y, z
	O3–H30···O2	0.89(5)	2.813(4)	2.04(5)	146	$-x, 3 - y, -z$
	C12–H12E···O1	0.94(3)	3.514(5)	2.60(3)	165	$-x, ½ + y, ½ - z$
II	O3–H30···O2	0.80(2)	2.648(2)	2.18(2)	117	x, y, z
	C9–H9A···O3	0.97(2)	3.124(2)	2.534(2	119	x, y, z
	C11–H11A···O3	0.98(2)	3.088(2)	2.436(2)	123	x, y, z
	C10–H10A···O1	0.96(2)	2.831(2)	2.32(2)	112	x, y, z
	O3–H30···O2	0.92(3)	2.867(2)	2.15(2)	149	$-x, -y, -z$
	C17–H17···O1	0.95(3)	3.323(2)	2.513(1)	142	$-x - 1, y - ½, -z + ½$
	C18–H18···Cl1	0.950(2)	3.651(2)	2.93(2)	133	$-x, -y - 1, -z + 1$
	Cg1···Cg2			3.829(1)		$x, ½ - y, -½ + z$
	Cg3···Cg1			3.759(1)		$x, -½ - y, ½ + z$
III	O3–H30···O2	0.89(5)	2.658(5)	2.25(4)	108	x, y, z
	C11–H11A···O1	1.10(5)	3.031(6)	2.39(5)	115	x, y, z
	C9–H9A···O1	1.05(6)	3.174(5)	2.57(2)	116	x, y, z
	O3–H30···O2	0.89(5)	2.854(5)	2.03(3)	154	$1 - x, 1 - y, 1 - z$
IV	O3–H30···O2	0.87(3)	2.641(2)	2.16(3)	115	x, y, z
	C9–H9A···O1	1.02(3)	3.119(3)	2.51(2)	118	x, y, z
	O3–H3O···O2	0.87(3)	2.843(3)	2.04(3)	154	$-x, 2 - y, -z$
V	C10–H10A···Cl1	0.95(3)	3.085(4)	2.60(3)	112	x, y, z
	C11–H11A···O1	0.92(3)	2.988(5)	2.37(3)	124	x, y, z
	C6–H6···Cl1	0.93(3)	3.758(4)	2.870(3)	160	$x + ½, ½ - y, z + ½$
VI	C9–H9A···O1	1.01(3)	3.124(5)	2.56(3)	115	x, y, z
	C10–H10···Cl1	0.99(3)	3.085(3)	2.52(3)	116	x, y, z
	C11–H11A···O1	0.91(3)	3.087(4)	2.52(3)	121	x, y, z
	C18–H18···Cl2	0.93(4)	3.659(5)	2.83(4)	150	$1 - x, -y, -z$
	C16–H16···O1	0.93(3)	3.419(5)	2.64(3)	140	$-x + 1, -y + 2, -z + 2$
	C2–H2···O2	0.909(4)	3.458(6)	2.63(4)	151	$x, +y, z - 1$
	Cg1···Cg1		3.986(3)			$2 - x, 1 - y, 1 - z$
VII	C9–H9A···O4	1.01(3)	3.167(5)	2.58(3)	116	x, y, z
	C10–H10···N1	0.94(3)	2.898(4)	2.39(2)	114	x, y, z
	C11–H11···O4	1.01(3)	3.102(5)	2.54(3)	115	x, y, z
	C31–H31A···O7	0.95(3)	3.115(5)	2.58(3)	116	x, y, z
	C32–H32···N2	0.95(3)	2.896(4)	2.39(3)	114	x, y, z
	C33–H33A···O7	0.96(3)	3.123(5)	2.56(3)	117	x, y, z
	C5–H5···O1	0.99(4)	3.546(5)	2.56(4)	172	$-x, 1 - y, 1 - z$
	C38–H38···O4	0.99(4)	3.335(5)	2.51(4)	141	$-x, 1 - y, 1 - z$
	C40–H40···Cl1	0.93(3)	3.635(4)	2.82(3)	146	$-x, 1 - y, 1 - z$
	C18–H18···Cl2	0.98(1)	3.781(4)	2.863(3)	156	$-x, 1 - y, 1 - z$

[a] Cg1 = centroid of the ring C1–C2–C3–C4–C5–C6, Cg2 = Centroid of C13–C14–C15–C20–C21–C22, Cg3 = centroid of C15–C16–C17–C18–C19–C20.

whereas, it is replaced by a NO_2 group in nitro atovaquone (**VII**). This ensures the absence of the formation of O–H···O intermolecular dimers and it is intended to study the flexibility of the molecule at the binding site with weaker perspective interactions in place of strong O–H···O hydrogen bonds. Fig. S5 and S6, ESI,† show the ORTEP diagram for the structures **V**,

Table 5 Inter ligand protein interaction and corresponding docking energy for atovaquone derivatives in the ubiquinol oxidation pocket

								VII	
	I	**IA**	**II**	**III**	**IV**	**V**	**VI**	**VIIA**	**VIIB**
O2···N–His181 (Å)	2.72	2.61	—	2.64	3.47	2.70	2.93	—	3.06
O1···OH_2 (Å)	2.58	2.53	2.70	2.51	2.45	2.79	2.50	2.61	2.69
Cl1···Thr122, OG1(Å)	3.33	3.86	—	—	—	3.30	4.04	—	—
NO···N–His181								2.50	2.57
O3···N–His181 (Å)	—	—	3.08		3.02	—	—	—	—
H_2O···Glu272, OE2 (Å)	2.61	2.61	2.61	2.61	2.61	2.61	2.61	2.61	2.61
Docking energy (kcal mol^{-1})	−7.81	−8.05	−10.12	−7.57	−9.50	−5.88	−7.25	−8.11	−7.89

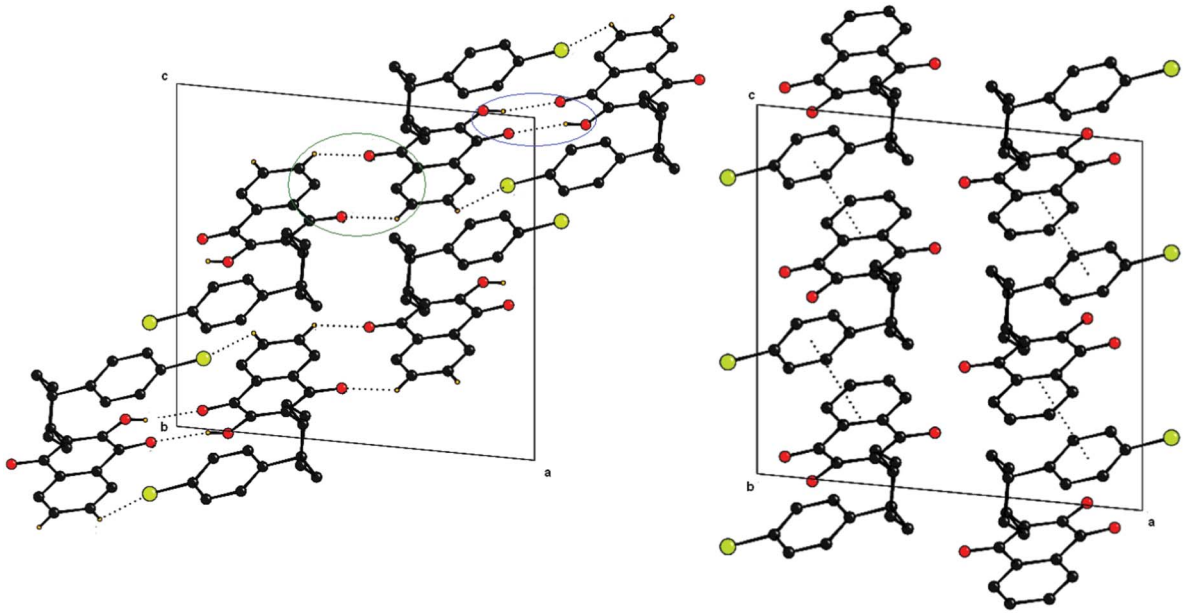

Fig. 4 The packing diagram of (**II**) *via* C–H···Cl, C–H···O (green circle) and O–H···O (blue circle) hydrogen bond and π···π interactions.

VI, and **VII** respectively. The molecular packing of *trans*-chloro atovaquone (**V**) is through weak C–H···Cl hydrogen bonds, whereas *cis*-chloro atovaquone (**VI**) forms dimers through C–H···O and C–H···Cl interactions along with an additional halogen···halogen [Cl···Cl = 3.39(2) Å), $\theta_1 = 170^\circ$, $\theta_2 = 132^\circ$, type II] interaction[44] stabilizing the packing of the molecule in the unit cell (Fig. 6). Nitro atovaquone (**VII**) packs the molecules with the dimer formation using C–H···O and C–H···Cl hydrogen bonds. In addition, molecular chains of halogen bonding,[48] [Cl···O = 3.26(1) Å, type II, $\theta_1 = 173^\circ$,$\theta_2 = 97^\circ$] provide further stability to the molecular assembly (Fig. 7). The effective conformational changes and the corresponding intermolecular interactions are given in Tables 2–4. Fig. 8 shows an overlap diagram of the molecular conformation of all the compounds with respect to the naphthoquinone ring.

Feature of atovaquone docking at the active site

The results show significant deviation from the computational model reported by Kissl *et al.*[26] The nature of bonding at the ubiquinol oxidation pocket differs significantly for each crystal

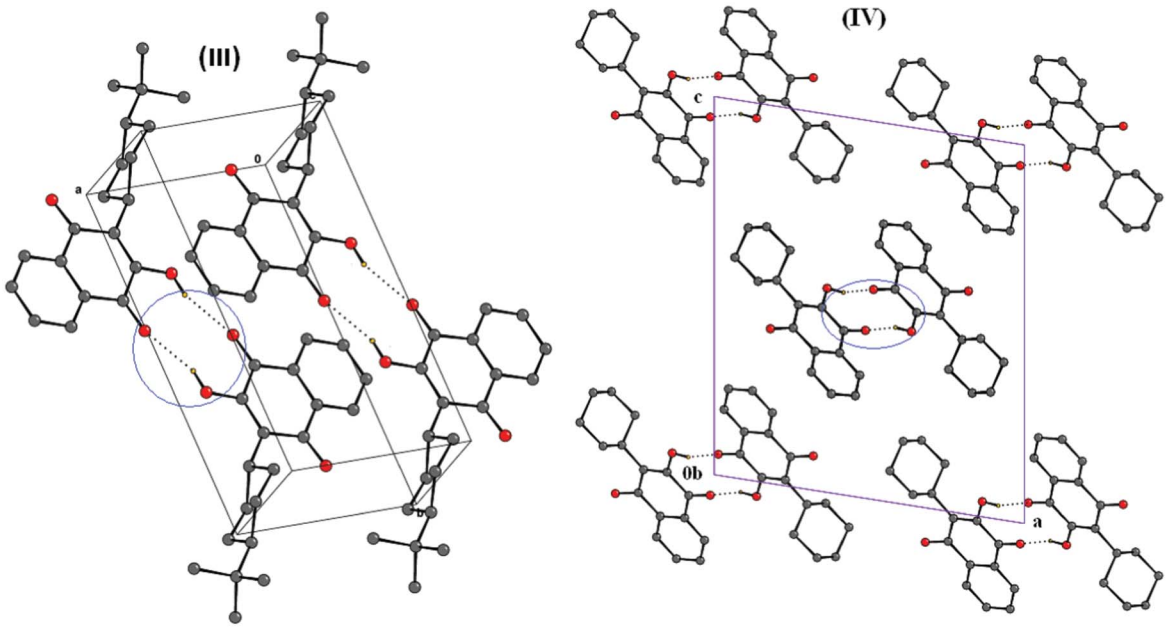

Fig. 5 Molecular dimer of (**III**) and (**IV**) *via* O–H···O hydrogen bonds (blue circle) viewed along *a*-axis.

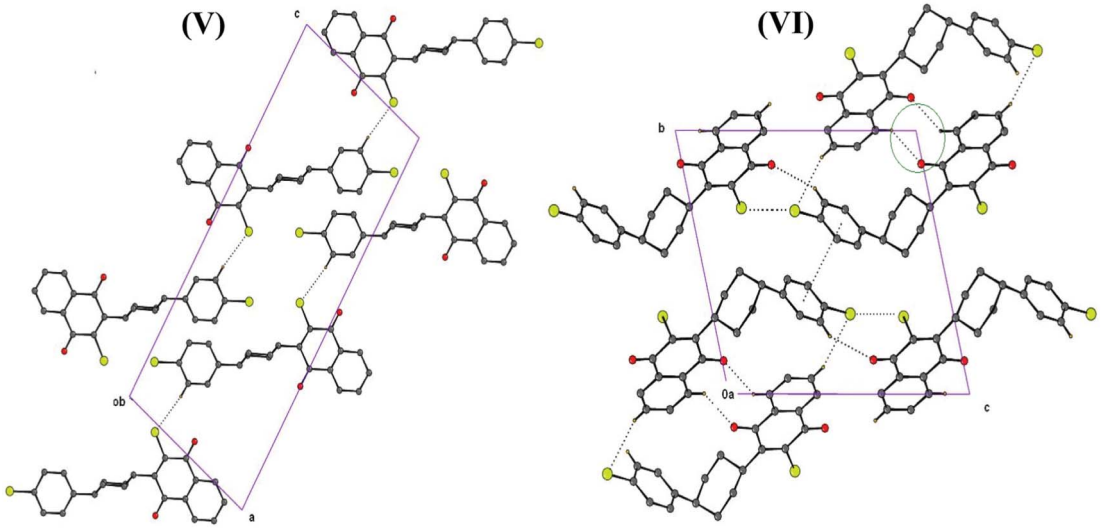

Fig. 6 The molecular chain (**V**) *via* C–H···Cl interactions and the packing of (**VI**) are mainly through C–H···O dimer (green circle), C–H···Cl, Cl···Cl, interactions and π···π stacking.

structure. Table 5 shows the feasible protein–ligand interactions and their docking energy. In *trans*-atovaquone (**I**), the keto group adjacent to the hydroxyl group forms a hydrogen bond with the NH of His181, whereas in the previous binding study on optimized structure,[26] it is the hydroxyl group that forms a hydrogen bond with the nitrogen atom of the imidazole group of the residue His181. The second keto group preferred to hydrogen bond with Glu272 through the active site water molecule (Table 5; Fig. 9). It is to be noted that the hydroxyl group of the ligand appears to retain the strong intramolecular hydrogen bonded feature observed in the crystal structure. Another interesting feature is the participation of the chlorine atom of the ligand forming O–H···Cl hydrogen bond through the hydroxyl group of Thr122 (Table 5; Fig. 9). Thus, the naphthoquinone ring fits into a polar cavity surrounded by the residues Tyr279, Arg283 and Pro271. However, the importance of the chlorine atom as a weak hydrogen bond had not taken into account in the previous study.[26] The hydrophobic chloro benzene moiety of the ligand molecule is surrounded by several hydrophobic residues Phe296, Ile299 and, Leu300 allowing the *trans*-atovaquone to be accommodated in the ubiquinol oxidation pocket. However, it may be noted that there is no indication of π···π interactions near the chloro benzyl moiety. The polymorphic form atovaquone (**IA**) results in a similar binding feature (Fig. 9; Table 5) with overall the same docking energy suggesting its biological significance.

In *cis*-atovaquone (**II**), the chloro benzene group folds into the region of overlap between the polar cavity and hydrophobic groups. However, the hydrogen bonding pattern of the ligand

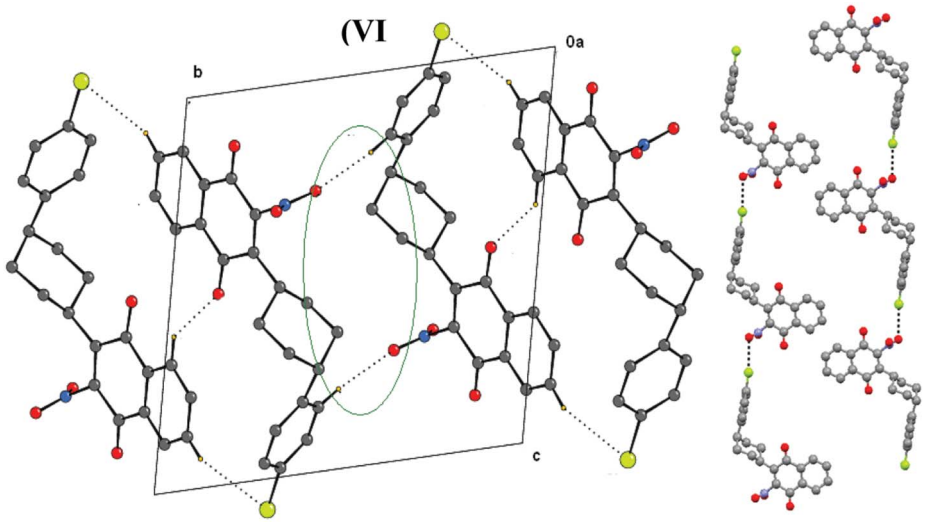

Fig. 7 The molecular packing of (**VII**) through molecular chain *via* Cl···O interactions, C–H···O dimer (green circle) and C–H···Cl hydrogen bonds.

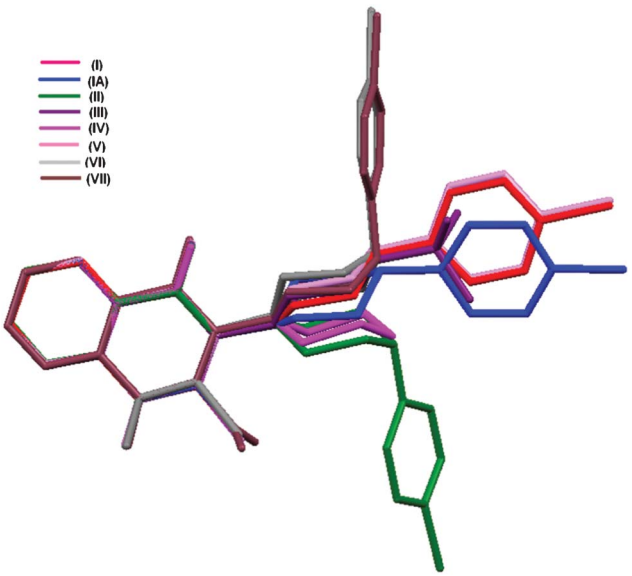

Fig. 8 Overlay diagram depicting the molecular conformation of all the compounds with respect to the naphthoquinone ring.

molecule with the protein is reversed. The hydroxyl group of the ligand molecule is hydrogen bonded with the nitrogen atom of the imidazole group of the residue His181 (Fig. 10), in a similar manner to that of the previous binding study on optimized structures of atovaquone (*trans*-atovaquone).[26] The chloro benzyl group of the ligand is far apart from Thr122 without involvement of any interaction unlike the O–H···Cl hydrogen bond in the case of **I** and **IA** due to their preferred conformation. However, the chloro benzyl group in this conformation faces the hydrophobic pocket of the residues Phe296, Ile299 and, Leu300, and contributes to strong ligand binding with the highest binding energy among all the molecules considered in this study (Table 5).

Tert-butyl atovaquone (**III**) has features similar to that of *trans*-atovaquone (Fig. 11), however the heavy *tert*-butyl group does not introduce any specific interactions other than pure van der Waals interactions resulting in a very low binding energy (Table 5). The absence of the chloro benzene moiety in parvaquone (**IV**) allows for the free movement in the binding pocket of the protein molecule (Fig. 11). The loss of the chloro benzyl group allows the molecule to form a bifurcated hydrogen bonding with the help of both its hydroxyl and keto group of the naphthoquinone ring with an equal possibility. Fig. 12 shows the differences in hydrogen bonding pattern between *trans*-chloro atovaquone (**V**) and *cis*-chloro atovaquone (**VI**). It is of interest to note that even on replacing the hydroxyl group by chloro substituent, the overall binding characteristic remains unaltered from those observed in **I** and **IA**. In *cis*-chloro atovaquone (**VI**), the chloro benzyl group resides 1.2 Å far away from Thr122 compared to *trans*-chloro atovaquone (**V**), which offers the possibility of altering the substitution at the hydroxyl site by both electron-withdrawing and electron-donating groups, for example, the structure of nitro atovaquone (**VII**) clearly offers a variant. One of the oxygen atoms of the nitro group forms strong hydrogen bonds with the residue His181. As expected, an equivalent energy conformation is observed with the possibility of bifurcated hydrogen bonding involving the keto group of the naphthoquinone moiety (Fig. 13) with an equal binding energy. Fig. 14 shows the comparison of all the binding modes of the molecules considered during the docking study. The impor-

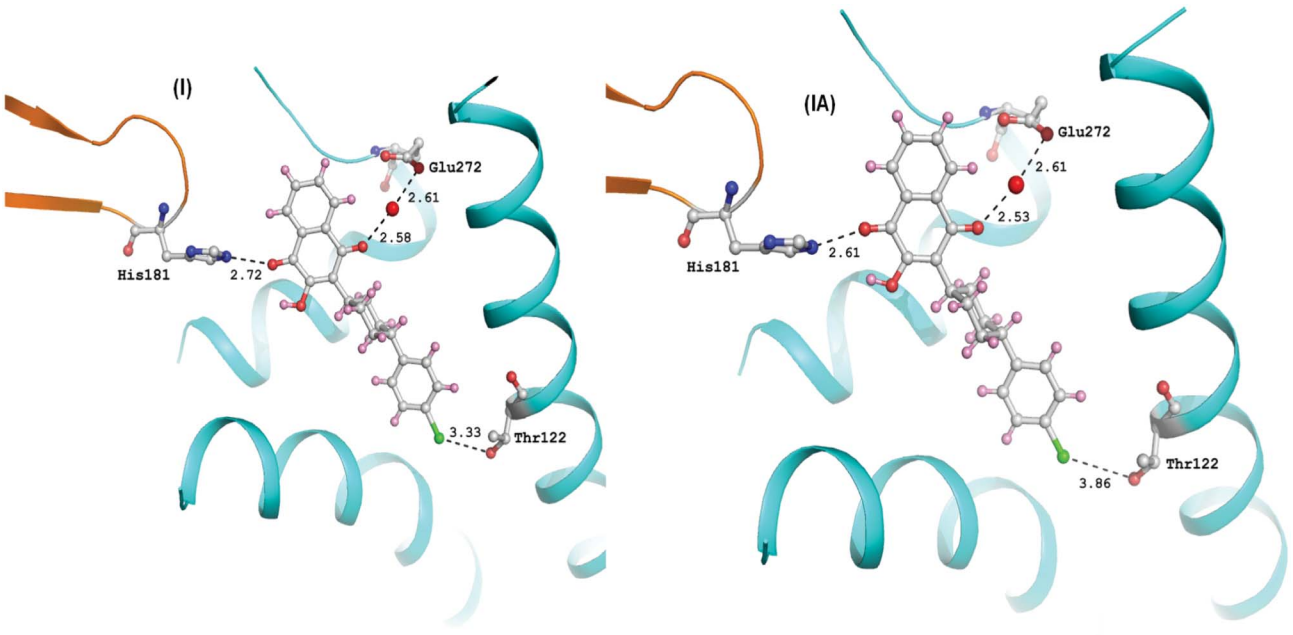

Fig. 9 Active sites of cytochrome bc_1 have been highlighted which shows the atovaquone (**I**, **IA**) binds to His181, Glu272 through a water molecule and Thr122. The hydrogen bond distances are labeled (shown with dotted lines).

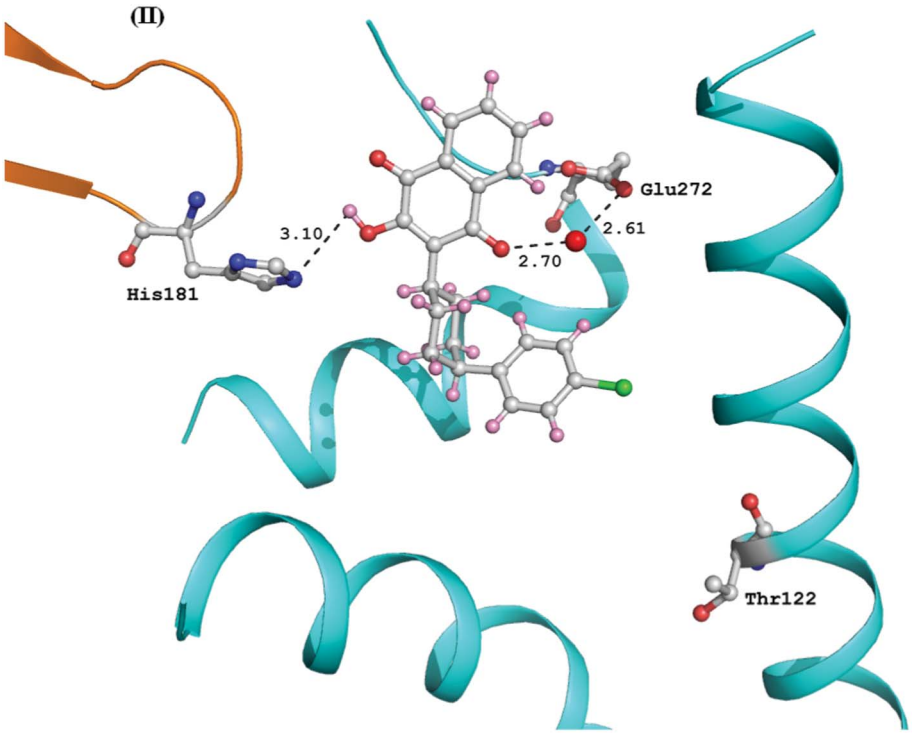

Fig. 10 The perspective view of *cis*-atovaquone with binding with the active site of cytochrome bc_1.

tance of hydrogen bonding of the residue His181 of the Rieske protein of one side and the interaction with the residue Glu272 on the other hand through a water molecule appears to be an essential factor irrespective of the ligand conformational variation. The strategy of keeping the active site water molecule, as suggested earlier,[26] allows the formation of the interaction due to the naphthoquinone carbonyl group and the carboxylate oxygen atom of Glu272. Furthermore, the rotation of Glu272 is an agreement of crystal structure of HDBT-bound yeast bc_1 complex.[26,47] Fig. 15 shows the minimized structure of atovaquone to the ubiquinol oxidation pocket of yeast bc_1 complex.

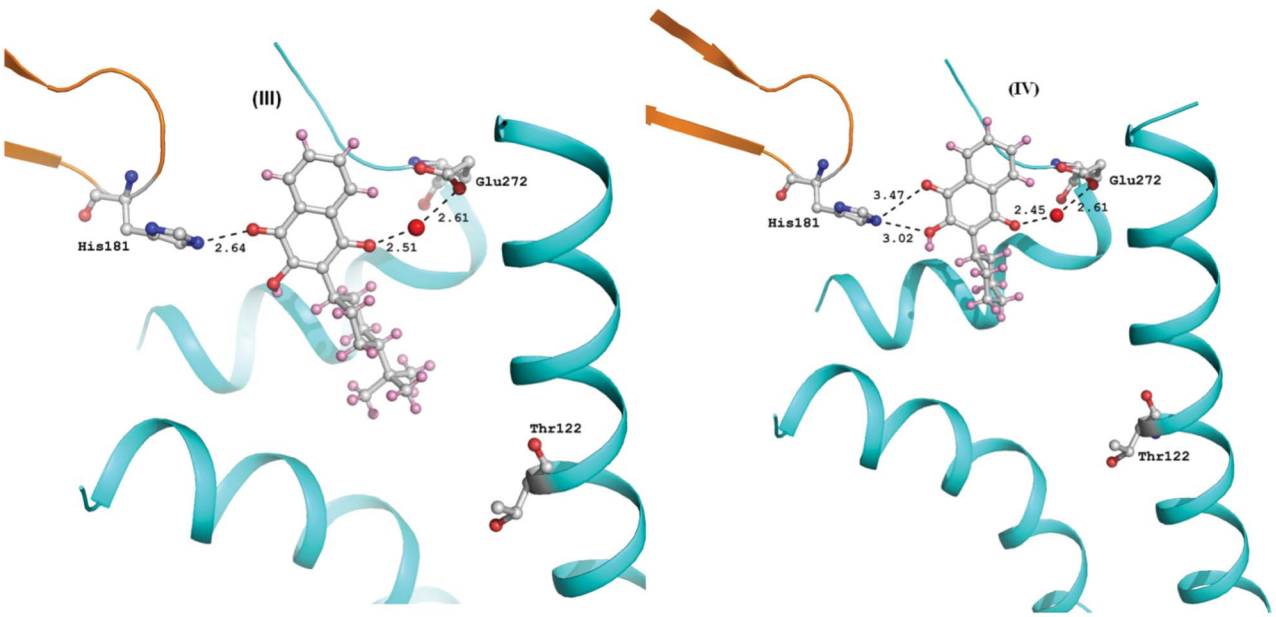

Fig. 11 Hydrogen bonding interaction of docked *tert*-butyl atovaquone (**III**) and parvaquone (**IV**) in their binding modes with cytochrome bc_1 shown separately.

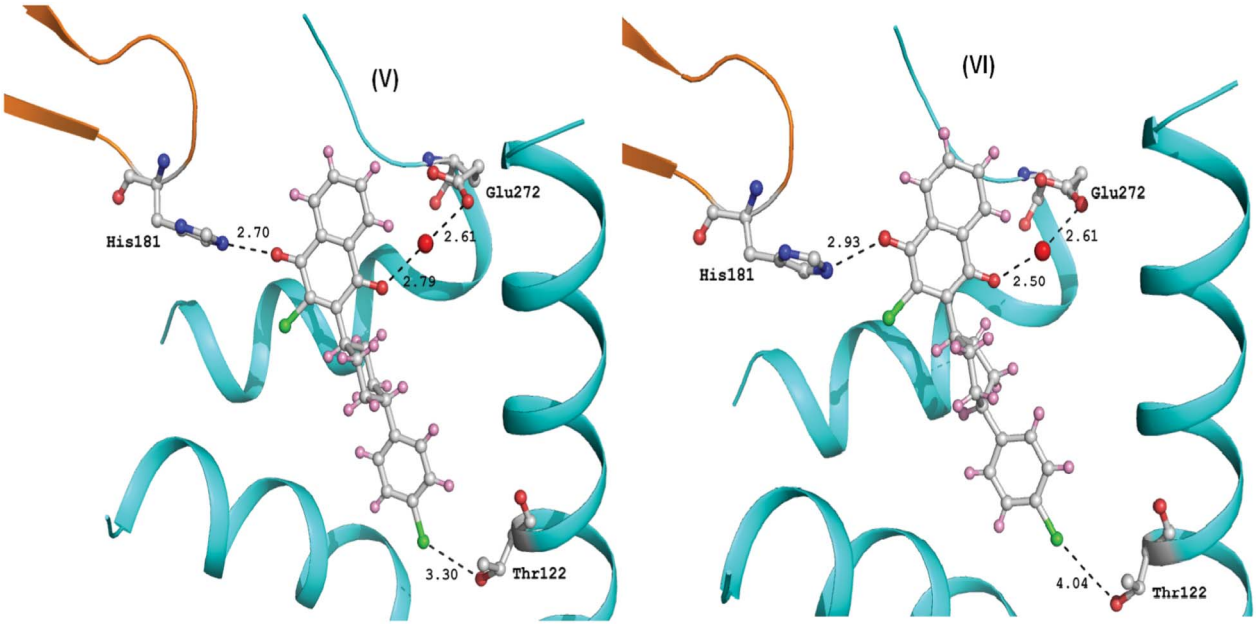

Fig. 12 Hydrogen bonding interaction of docked *trans*-chloro atovaquone (**V**) and *cis*-chloro (**VI**) atovaquone in their binding modes with cytochrome bc_1 shown separately.

Cytochrome bc_1 complex exists as a dimer with each half of the dimeric complex having a binding site for ubiquinol/ubiquinone which is inhibited by quinone type of drugs such as stigmatellin and atovaquone. Of the two electrons released during the ubiquinol oxidation one goes to the heme group of cytochrome bc_1 through the Rieske iron–sulfur protein, which is involved in the mitochondrial electron transfer path. The key issue for such electron transfer is the formation of strong hydrogen bonding of the histidine residue with ubiquinone.[45,46] The second electron reconverts ubiquinone to ubiquinol. This electron transfer takes place through the protein residue of cytochrome b_{562}. The strong hydrogen bonding with the glutamic acid is the key point in this pathway. Ubiquinone binding to cytochrome bc_1 by these two main strong hydrogen bonds is mimicked in the case of the stigmatellin complex suggesting it to be a potential inhibi-

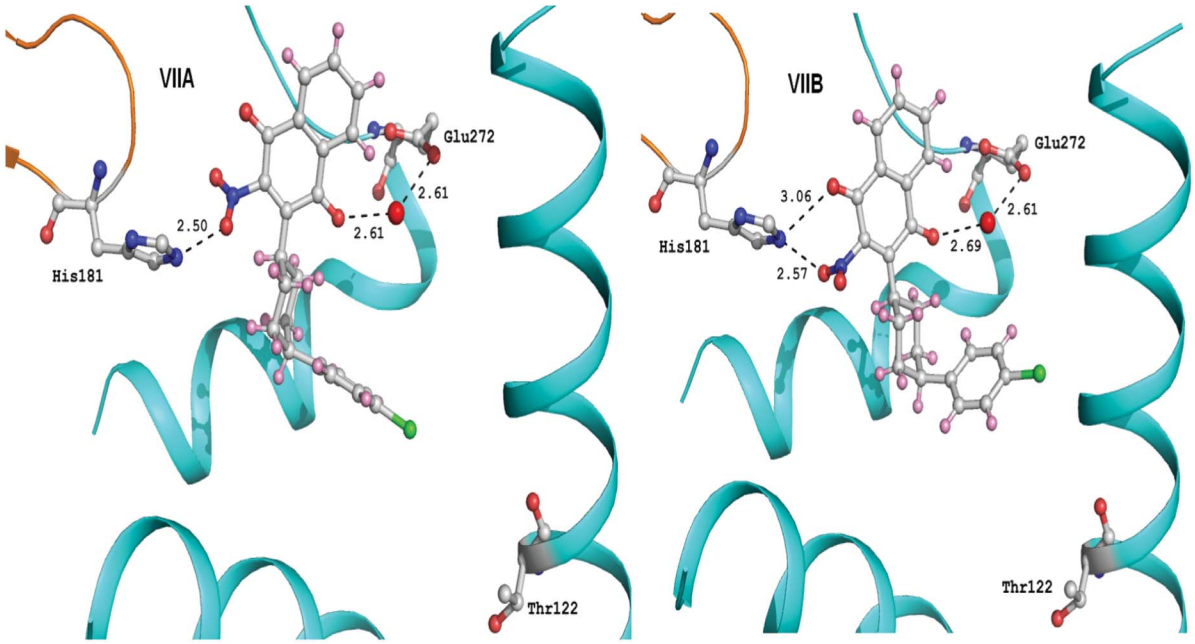

Fig. 13 Hydrogen bonding interaction of two different equally possible conformations of nitro-atovaquone (**VIIA** and **VIIB**) with cytochrome bc_1 separately.

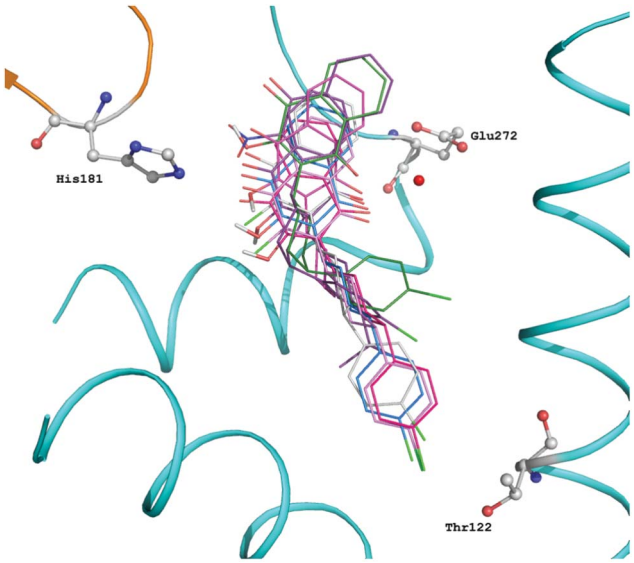

Fig. 14 The clusters of docked atovaquones in the active site of cytrochrome bc_1 complex.

tor.[24] It is noteworthy that atovaquone and its derivative studied in the present work, show better binding to the protein molecule. Furthermore, it is stabilized by water molecule hydrogen bonded to Glu272 in the active site. Interestingly, the ligand molecules docked with the cytochrome bc_1 complex occupy the active site cavity.

The detailed structural studies presented above clearly suggest that the requirement of the drug conformation lies in the formation of intra and intermolecular hydrogen bonds and the propensity of the molecules to pack with dimer configurations involving strong O–H···O hydrogen bonds. The presence of weak interactions like C–H···O and C–H···Cl along with Cl···Cl and Cl···O contacts provide the possible variations in the nature of packing motifs that can be examined further

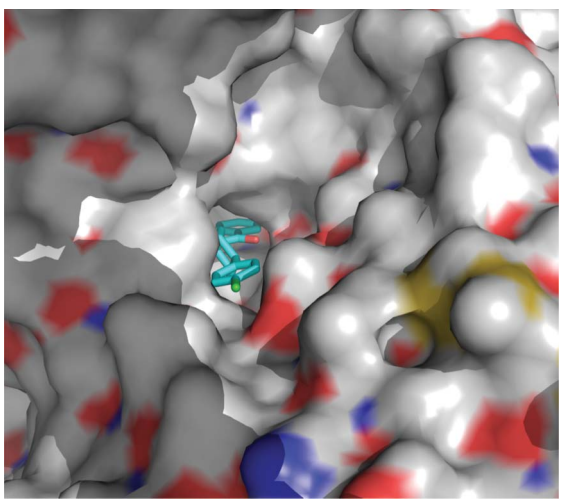

Fig. 15 The energy minimized structure of atovaquone to the ubiquinol oxidation pocket of yeast bc_1 complex.

for variability in drug behavior. The additional feature of π-stacking also suggests the possibility of checking such derivatives in selective docking with the protein. In fact, the occurrence of two polymorphs of atovaquone provides a platform to examine the binding characteristics and allows for a careful scrutiny of these structures as efficient drugs in terms of their bioavailability and functionality. It must be pointed out that the conformation as found in the crystal structure of both polymorphs are very different to that of modeled stigmatellin as suggested in the previous study.[24,26]

Using theoretically optimized coordinates, it has been shown that the residue Glu272 is involved in the binding of the atovaquone molecule through a water molecule.[26] The structure determination of atovaquones followed by the docking studies of these compounds with the cytochrome bc_1 complex provides insights into the binding mode of the molecules in the active site of the protein molecule. The polymorph (**IA**) shows the shorter hydrogen bonds to the residues Glu272 and His181 suggesting the possibility of a better binding characteristics. *cis*-Atovaquone (**II**) reveals the binding of the ligand molecule through the hydroxyl group with the residue His181 with the highest binding energy (-10.12 kcal mol^{-1}) among all the molecules considered. The binding energy of *trans*-chloro atovaquone (**V**) is least (-5.88 kcal mol^{-1}), possible due to the preference of weak hydrogen bond (2.79 Å, Table 5; Fig. 12) of keto group to the water molecule compared to other derivatives of atovaquone.

Conclusion

Atovaquone and its derivatives owing to their nature of hydrogen bonding interactions and the propensity towards the formation of weaker hydrogen bonds involving the chlorine atom, appear to be a potential candidate drug for further evaluation. The conformation of the molecules in the crystal structure in almost all the cases is influenced by the possibility of dimer formation. It is noteworthy that these studies clearly established that crystal engineering methodologies in combination with docking studies allow for inhibitor design and hence provide pointers to the discovery of new drugs. This area needs further examination supported by additional *in situ* biochemical and animal experimentation thus opening up new vistas towards the understanding of drug design.

Acknowledgements

We thank DST, India for the XRD facility at IISc and SKN thanks CSIR & DST for fellowship and financial support. TNG thanks DST for the award of J. C. Bose fellowship.

References

1 R. W. Snow, C. A. Guerra, A. M. Noor, H. Y. Myint and S. I. Hay, *Nature*, 2005, **434**, 214–217.

2 (*a*) C. L. A. Laveran, B. H. Kean, K. E. Mott and A. J. Russell, *Clin. Infect. Dis.*, 1982, **4**, 908–911; (*b*) R. Ross, *Yale J. Biol. Med.*, 2002, **75**, 103–105.
3 R. Ramzi, S. Cotran, V. Kumar, T. Collins, S. L. Robbins and B. Schmitt, *Pathologic Basis of Disease*, W. B. Saunders, New York, 6th edn, 1999.
4 S. Jarcho, *Quinine's Predecessor: Francesco Torti and the Early History of Cinchona*, Johns Hopkins University Press, Baltimore and London, 1993.
5 (*a*) C. Wongsrichanalai, A. L. Pickard, W. H. Wernsdorfer and S. R. Meshnick, *Lancet Infect. Dis.*, 2002, **2**, 209–218; (*b*) W. Peters, *Adv. Parasitol.*, 1998, **41**, 19–62; (*c*) H. Unsuren, A. Kurtdede and K. Gokus, *Trop. Anim. Health Prod.*, 1988, **20**, 256–258; (*d*) H. A. Mbwambo, F. F. Sudi, P. A. Mkonyi, J. M. Mfinanga, E. S. Mella and C. J. Ngovi, *Vet. Parasitol.*, 2002, **108**, 195–205; (*e*) E. Forestier, A. Labe, D. Raffenot, C. Lecomte and O. Rogeauxa, *Med. Mal. Infect.*, 2011, **41**, 41–43.
6 A. Dorn, S. R. Vippagunta, H. Matile, C. Jaquet, J. L. Vennerstrom and R. G. Ridley, *Biochem. Pharmacol.*, 1998, **55**, 727–736.
7 R. Banerjee, J. Liu, W. Beatty, L. Pelosof, M. Klemba and D. E. Goldberg, *Proc. Natl. Acad. Sci. U. S. A.*, 2002, **99**, 990–995.
8 T. J. Egan, D. C. Ross and P. A. Adams, *FEBS Lett.*, 1994, **352**, 54–57.
9 A. F. G. Slater and A. Cerami, *Nature*, 1992, **355**, 167–169.
10 A. V. Pandey, V. K. Babbarwal, J. N. Okoyeh, R. M. Joshi, S. K. Puri, R. L. Singh and V. S. Chauhan, *Biochem. Biophys. Res. Commun.*, 2003, **308**(4), 736–743.
11 A. Yayon, Z. I. Cabantchik and H. Ginsburg, *Proc. Natl. Acad. Sci. U. S. A.*, 1985, **82**, 2784–2788.
12 A. B. S. Sidhu, D. Verdier-Pinard and D. A. Fidock, *Science*, 2002, **298**, 210–213.
13 S. R. Meshnick, *Int. J. Parasitol.*, 2002, **32**, 1655–1660.
14 P. D. Mongan, J. J. Karaian, D. Dubois, R. Keneally and P. Sharma, *Am. J. Physiol.*, 2002, **283**, H1634–H1644.
15 D. J. Walker, J. L. Pitsch, M. M. Peng, B. L. Robinson, W. Peters, J. Bhisutthibhan and S. R. Meshnick, *Antimicrob. Agents Chemother.*, 2000, **44**, 344–347.
16 H. Myllykallio, D. Leduc, J. Filee and U. Liebl, *Trends Microbiol.*, 2003, **11**, 220–223.
17 G. J. C. Basset, E. P. Quinlivan, J. F. Gregory and A. D. Hanson, *Crop Sci.*, 2005, **45**, 449–453.
18 (*a*) R. G. Ridley, *Nature*, 2002, **415**, 686–693; (*b*) M. Chen, N. Korsinczky, B. Kotecka, A. Saul, K. Rieckmann and Q. Cheng, *Antimicrob. Agents Chemother.*, 2000, **44**, 1765.
19 E. Fontaine, F. O. Ichas and P. Bernardi, *J. Biol. Chem.*, 1998, **273**, 25734–25740.
20 http://people.ok.ubc.ca/wsmcneil/bio/electronchain.htm.
21 A. G. M. Tielens and J. J. V. Hellemond, *Biochim. Biophys. Acta, Bioenerg.*, 1998, **1365**, 71–78.
22 A. Kroger and M. K. Gwith, *Eur. J. Biochem.*, 1973, **34**, 358–368.
23 I. K. Srivastava, J. M. Morrisey, E. Darouzet, F. Daldal and A. B. Vaidya, *Mol. Microbiol.*, 1999, **33**, 704–711.
24 B. Kunze, T. Kemmer, G. Hofle and H. Reichenbach, *J. Antibiot.*, 1984, **37**, 454–461.
25 C. Hunte, J. Koepke, C. Lange, T. Rossmanith and H. Mitchel, *Structure*, 2000, **8**, 669–684.
26 (*a*) J. J. Kessl, B. B. Lange, T. Merbitz-Zahradnik, K. Zwicker, P. Hill, B. Meunier, H. Pálsdóttir, C. Hunte, S. Meshnick, B. Meunier and B. L. Trumpower, *J. Biol. Chem.*, 2003, **278**, 31312–31318; (*b*) J. J. Kessl, P. Hill, B. B. Lange, S. R. Meshnick, B. Meunier and B. L. Trumpower, *J. Biol. Chem.*, 2003, **279**, 2817–2824; (*c*) S. Looareeuwan, J. D. Chulay, C. J. Canfield and D. B. A. Hutchinson, *Am. J. Trop. Med. Hyg.*, 1999, **60**, 533–541.
27 (*a*) G. Klebe, *J. Mol. Med.*, 2000, **78**, 269–281; (*b*) F. Colizzi, R. Perozzo, L. Scapozza, M. Recanatini and A. Cavalli, *J. Am. Chem. Soc.*, 2010, **132**, 7361–7371; (*c*) A. C. Anderson, *Chem. Biol.*, 2003, **10**, 787–797.
28 D. R. Williams and M. P. Clark, *Tetrahedron Lett.*, 1998, **39**, 7629–7632.
29 (*a*) V. S. Latter and W. E. Gutteridge, *US Pat.*, 4981874, Jan. 1, 1991; (*b*) A. T. Hudson and A. W. Randall, *US Pat.*, 4485117, Nov. 27, 1984.
30 SMART (V 5.628), SAINT (V 6.45a), SADBS, XPREP, SHELXTL, Bruker AXS Inc., Madison, WI, 2004.
31 G. M. Sheldrick, *Acta Crystallogr., Sect. A: Found. Crystallogr.*, 2008, **A64**, 112–122.
32 L. J. Farrugia, *J. Appl. Crystallogr.*, 1999, **32**, 837–838.
33 L. J. Farrugia, *J. Appl. Crystallogr.*, 1997, **30**, 565–566.
34 D. M. Watkin, L. Pearce and C. K. Prout, CAMERON – A Molecular Graphics Package, Chemical Crystallography Laboratory, University of Oxford, Oxford, 1993.
35 M. Nardelli, *J. Appl. Crystallogr.*, 1995, **28**, 659.
36 A. L. Spek, *Acta Crystallogr., Sect. A: Found. Crystallogr.*, 1990, **A46**, c34.
37 G. M. Morris, D. S. Goodsell, R. Huey, W. E. Hart, R. S. Halliday, R. K. Belew and A. J. Olson, Autodock, Version 3.0.5, Department of Molecular Biology, Molecular Graphics Laboratory, The Scripps Research Institute, La Jolla, CA, 2001.
38 http://www.rcsb.org.
39 P. Emsley and K. Cowtan, Coot: model-building tools for molecular graphics, *Acta Crystallogr., Sect. D: Biol. Crystallogr.*, 2004, **D60**, 2126–2132.
40 A. W. Schüttelkopf and D. M. F. van Aalten, PRODRG: a tool for high-throughput crystallography of protein-ligand complexes, *Acta Crystallogr., Sect. D: Biol. Crystallogr.*, 2004, **D60**, 1355–1363.
41 F. J. Solis and R. J. B. Wets, *Math. Oper. Res.*, 1981, **6**, 19–30.
42 G. Syswerda, Uniform crossover in genetic algorithms, *Proceedings of the Third International Conference on Genetic Algorithms*, ed. J. D. Schaffer, Morgan Kaufmann, 1998.
43 W. D. Delano and S. Bromberg, *PyMOL User's Guide*, 2004.
44 (*a*) G. R. Desiraju and R. Parthasarathy, *J. Am. Chem. Soc.*, 1989, **111**, 8725–8726; (*b*) T. T. T. Bui, S. Dahaoui, C. Lacomte, G. R. Desiraju and E. Espinosa, *Angew. Chem., Int. Ed.*, 2009, **48**, 3838–3841; (*c*) S. K. Nayak, S. J. Prathapa and T. N. Guru Row, *J. Mol. Struct.*, 2009, **935**, 156–160; (*d*) S. K. Nayak, M. K. Reddy, T. N. Guru Row and D. Chopra, *Cryst. Growth Des.*, 2011, **11**, 1578–1596.
45 Z. Zhang, L. Huang, V. M. Shulmeister, Y. Chi, K. K. Kim, L. Hung, A. R. Croftsk, E. A. Berry and S. Kim, *Nature*, 1998, **392**, 677–684.
46 P. Michell, *J. Theor. Biol.*, 1976, **62**, 327–367.
47 H. Palsdottir, C. G. Lojero, B. L. Trumpower and C. Hunte, *J. Biol. Chem.*, 2003, **278**, 31303–31311.

48 P. Metrangolo, F. Mayer, T. Pilati, G. Resnati and G. Terraneo, *Angew. Chem., Int. Ed.*, 2008, **47**, 6114–6127.
49 L. Malpezzi, C. Fuganti, E. Maccaroni, N. Masciocchi and A. Nardi, *J. Therm. Anal. Calorim.*, 2010, **102**, 203–210.
50 (*a*) D. Dinter, G. Gajski and V. Garaj-Vrhovac, *J. Appl. Toxicol.*, 2013, **33**, 56–62; (*b*) E. Wallace, C. M. Ong and C. M. Heard, *Pharm. Dev. Technol.*, 2012, **17**, 770–776; (*c*) H. Britton, D. Catterick, A. N. Dwyer, A. H. Gordon, S. G. Leach, C. McCormick, C. E. Mountain, A. Simpson, D. R. Stevens, M. W. J. Urquhart, C. E. Wade, J. Warren, N. F. Wooster and A. Zilliox, *Org. Process Res. Dev.*, 2012, **16**, 1607–1617; (*d*) A. Mavrogordato and A. M. Lever, *J. Infect.*, 2012, **65**, 269–274 and references therein.

